

Optimal Bass Reflex Loudspeaker Port Design

A. Bezzola¹

1. DMS Audio Lab, Samsung Research America, Valencia, CA, USA

Abstract

Turbulence and vortex shedding in ports of bass reflex loudspeaker systems can produce noise at high sound-pressure levels. Flared ports can reduce port noise compared to straight ports, but the optimal amount of flare in ports has remained an unsolved problem. This work shows that solutions to the Helmholtz equation can be used to design ports that have low propensity for vortex shedding and therefore have low noise levels. Optimality of the port design is validated with measurements and double-blind listening tests of several prototypes. Results show that optimally designed ports can be played 1 to 3 dB louder than slightly under- or over-flared ports, and 10 to 16 dB louder than straight unflared ports, before the unwanted port noise becomes audible.

Introduction

Sealed-box loudspeakers have limited low-frequency (bass) output because the excursion of the woofer diaphragm is limited by its suspension elements. Additionally, large woofer excursion can lead to strong non-linear distortion of the audio signal, reducing sound quality. Bass reflex ports improve the low-frequency performance of loudspeakers by adding an air mass in the port that resonates with the compliance of the air inside the loudspeaker enclosure to create a second mass-spring-damper (MSD) system. In a simple lumped-parameter model of the bass reflex loudspeaker, the two-MSD system can be tuned such that the woofer diaphragm excursion is reduced at port tuning frequency.

At low sound pressure levels (SPL) the air flow in the port remains laminar, extending the low-frequency output and improving the efficiency of the loudspeaker. As SPL increases so does the velocity of air within the port, which means the flow may become turbulent. Distortion, compression and noise artifacts rise dramatically with the onset of turbulence [1]. It has long been a goal to consistently design ports with minimal noise caused by turbulent flow. Experimental studies have shown that adding flanges and blend radii at the ends of the port significantly reduces port noise [2]. Experiments with continuously flared ports showed additional improvements [3, 4].

In 1998, Roozen et al. postulated that boundary layer turbulence and unsteady flow separation are the main culprit for unwanted port noise [5, 6, 7]. They numerically and empirically demonstrated that vortices shed at either end of the port tube, which generates an impulsive excitation to the air inside the port, resulting in unwanted port noise at the first port resonance. Their findings suggested that a port with

gentle flare and small blend radii at the ends has minimal noise.

The notion that gentle flares are optimal for low port noise was challenged when a series of ports was used in listening tests performed by Salvatti et al. [1]. They found that generous flares are optimal at low SPL and straight ports are optimal at extremely high SPL. Rapoport and Devantier [8] found that compression and distortion measurements of ports do not necessarily correlate with results from double-blind listening tests. However, unpublished listening tests data from [8] (to be published in [9]) suggests that there is an optimal amount of flare in a loudspeaker port, and that over- and under-flared ports are rated lower by listeners in double-blind listening tests.

Several Computational Fluid Dynamics (CFD) studies have been published on the matter [10, 11, 12]. The numerically very costly simulations did not provide a solution to the problem of optimal flare rate in ports, but the work by Garcia-Alcaide et al. in [12] also observed vortex shedding and the resulting impulsive excitation of the port.

Flow Separation Theory and Port Noise

Several of the studies mentioned in the Introduction suggest that flow separation and vortex shedding generate unwanted noise that is most objectionable to listeners. Vortex shedding occurs when the air flow at the exit of the port tube is separating, creating a reversal of flow direction. Flow separation can be described by the stream-wise momentum equation of fluid flows:

$$u \frac{\partial u}{\partial s} = -\frac{dp}{ds} + \nu \frac{\partial^2 u}{\partial y^2} \quad (1)$$

where u is the velocity along stream lines and s is the streamwise coordinate, y is the normal coordinate, and ν is the viscosity. Flow reversal is primarily

caused by an adverse pressure gradient imposed in the boundary layer. An adverse pressure gradient is when shear stress $\frac{dp}{ds} > 0$, which can be seen to cause the velocity u to decrease along s and possibly go to zero if the adverse pressure gradient is strong enough as illustrated in Figure 1.

While Equation (1) is typically used for flow separation in unidirectional flow in boundary layers, it offers a possible insight into how to optimize loudspeaker port tubes with bidirectional flow. Flow separation leads to vortex shedding, which can excite the air inside the port tubes with an impulse-like disturbance. This impulse excites all frequencies in the port, and most critically, it will excite the eigenfrequency of the air inside the port.

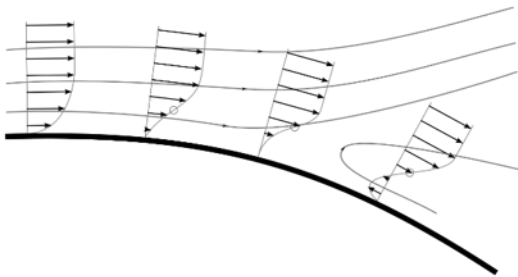


Figure 1. Graphical representation of the velocity profile in the boundary layer. The last profile represents adverse pressure gradient which results in separated flow. Continuous lines are streamlines and arrows are local velocity vectors. By Olivier Cleynen, licensed by CC BY 3.0.

Disregarding end corrections, the first eigenfrequency of ports f_p^1 occurs when the half-wavelength $\lambda/2$ is equal to the port length L .

$$f_p^1 = \frac{c}{\lambda} \approx \frac{c}{2L}, \quad (2)$$

where c is the speed of sound. For typical port lengths in bass reflex boxes below 0.5 m, f_p^1 is larger than 343 Hz, which is several octaves higher than typical port tuning frequencies in loudspeakers. When the port eigenfrequencies get excited by flow separation and vortex shedding, they are very audible to the human ear, because they are outside the spectral masking bandwidth of the nominal port operating frequencies. The unwanted “noise” that is associated with the port eigenfrequencies is often interpreted as turbulent air noise in ports. The word “noise” in this context is not related to a random signal like measurement noise, but rather expresses

the unwanted audible high-frequency content from a port that is driven at high levels.

The fluid flow in a loudspeaker port can be fully described by the Navier-Stokes (NS) equations. The NS equations describe momentum conservation in fluids, including fully turbulent flow, flow separation, and vortex shedding, but they are notoriously hard to solve. The NS equations can be linearized, and under the assumption of negligible viscosity and thermal conductivity, they can be formulated as the Linear Wave equation in the time domain, or the Helmholtz equation in the frequency domain, which are much easier to solve.

Designing an optimal loudspeaker port using the acoustic Helmholtz equation, can be thought of as the following problem:

“Which port profile has the lowest propensity to generate turbulence, flow separation, and vortex shedding”?

In this work, we hypothesize that the optimal port profile has the lowest amount of shear stress across the port exit. The hypothesis will be tested with acoustic measurements and blind listening tests.

Setup and Acoustic Simulations in COMSOL

The models were set up in COMSOL using the Acoustic Module for calculating the pressure distribution and particle velocity in the loudspeaker and port tube. A lumped parameter model of two 10-inch loudspeaker drivers was implemented as an LCR network in the “Electrical Circuit” interface of the AC/DC Module. The drivers were coupled to the acoustic interface as described in the COMSOL Application Library Model “Lumped Loudspeaker Driver.” The port was assumed to be mounted on the outside of the enclosure and the port mounting baffle was assumed to be infinite. In the far field, a Perfectly Matched Layer (PML) was used to ensure that acoustic waves are not reflected at the geometry boundary. A sketch of the setup and a close-up of the port and enclosure is shown in Figure 2.

Simulations of Ports from Rapoport and Devantier [8]

The first round of simulations was performed with the port geometries as listed in [8]. In addition to the ports named “B,” “C,” and “D” that are listed in the paper, Rapoport and Devantier later also tested a port named “E,” and showed the results at the 117th AES Convention in San Francisco. All the ports were tuned to 30 Hz in a 24.6 L enclosure. The dimensions

for the four ports are shown in Table 1. D_c is the central (minimal) diameter, D_e is the diameter at port exit (without blend radii applied), R_b is blend radius at port exits, and V_{box} is the volume of internal air of the enclosure. All ports were designed including a port exit flange with OD of 180 mm.

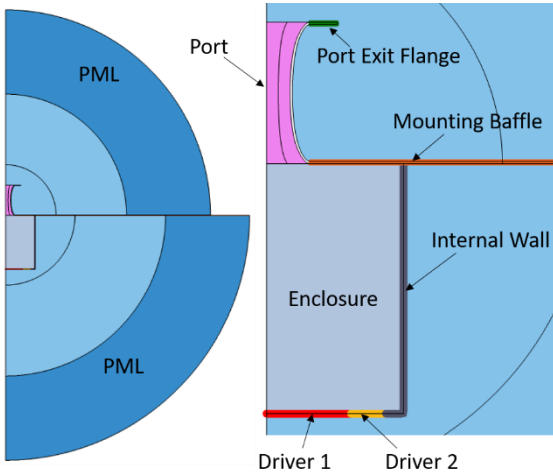


Figure 2. Axisymmetric model setup in COMSOL with close-up view of the port, baffle, enclosure and drivers on the right.

Table 1. Dimension of ports as listed in [8,9].

Port	B	C	D	E
Length [mm]	120	120	120	120
D_c [mm]	62.9	61.8	60.9	60.1
D_e [mm]	79.2	87.4	96.7	107
R_b [mm]	15	15	15	15
V_{box} [L]	24.6	24.6	24.6	24.6

Based on a series of double-blind listening test, the authors concluded that port “D” was the best port [9]. Linear acoustic simulations of the Helmholtz equation at port tuning frequency revealed an interesting phenomenon: the particle velocity contours at port exit transitioned from concave to convex with increasing flare rate, and port “D” had a near-flat particle velocity contour at port exit, as shown in Figure 3. This observation correlates with the idea of flow separation, because a flat velocity contour line at port exit indicates low shear stress and thus low propensity for flow separation.

Simulations of Ports with Different Aspect Ratios

The ports from the previous section all had a nominal aspect ratio of Length: D_c = 2:1. To test the hypothesis, eight additional ports were designed and prototyped. Five of the new ports had a nominal

aspect ratio of 3:1, and three had a nominal aspect ratio of 4:1.

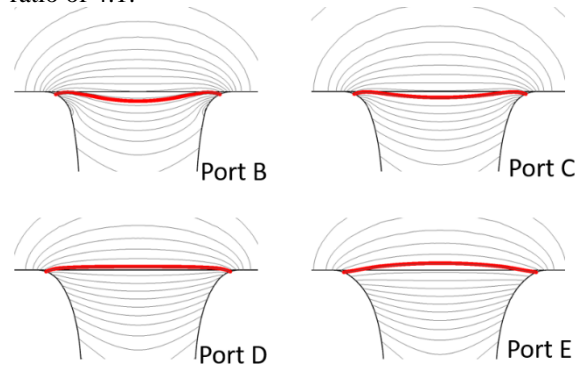


Figure 3. Particle velocity contours. Contours at port exit transition from concave to convex with increasing flare rate.

The following iterative method was used to find the suspected optimal port profile:

1. Fix D_c at 59 mm
2. Find box volume (V_{box}) to keep port tuning frequency at 40 Hz.
3. Optimize D_e and blend radius R_b until minimal curvature is observed in the velocity contours at port exit.
4. Repeat steps 2 and 3 until convergence is found.

After finding the optimal ports for each aspect ratio, four more ports were designed with central diameters of 57 mm and 61 mm respectively. R_b and V_{box} were kept constant for all ports with the same aspect ratio, but the flare rate was adjusted to result in a port tuning of 40 Hz for all ports. For the 3:1 aspect ratio, two additional ports were designed and prototyped: a straight port without flange and blends and a flanged straight port with blends at port exit. All flanged ports had a port exit flange with OD of 180 mm.

Setup for Optimizations

Three kinds of parameter optimizations [13] were needed to design all the ports. The first optimization was needed to find the box volume for a port with given D_c , D_e , Length, and R_b , so that port tuning is at the desired frequency of 40 Hz. This was done in COMSOL via an Acoustic Eigenfrequency step, combined with a Global Objective to minimize the square of the error between the simulated eigenfrequency and the desired port tuning frequency. The PML setting was set to have “Typical Wavelengths” set to the wavelength at 40 Hz. The optimization was run with a BOBYQA solver and typically converged very fast.

The second optimization was to optimize D_e and R_b for maximally flat particle velocity contours at port

exit, with fixed V_{box} , D_c , and Length. An integral Objective on the port exit boundary was set to minimize the variance of the particle velocity. The optimization solver was again BOBYQA.

The third kind of optimization was needed to find D_e for the over- and under-flared variants of the ports, such that they also tune to the desired 40 Hz, but with fixed V_{box} , D_c , R_b and Length. This was also done with an eigenfrequency simulation similar to the first optimization.

To streamline the process of running the three different kind of optimization problems, model methods were used in combination with a simple Settings Form in the COMSOL Model Builder. The form to drive the optimizations is shown in Figure 4. The resulting geometry parameters for the eight new ports are shown in Table 2, and the particle velocity contours are shown in Figures 5 and 6.

SimpleParametersForm

Desired Port Tuning:	<input type="text" value="40"/>	Hz
Port Length:	<input type="text" value="180"/>	mm
Vol_set:	<input type="text" value="30.61745001588E"/>	L
D_0 _set:	<input type="text" value="59.000000000000"/>	mm
Dexit_set:	<input type="text" value="117.0006683300E"/>	mm
rFillet_set:	<input type="text" value="8.4357341669361"/>	mm

Optimize Velocity Differential

Optimize Tuning by Volume

Optimize Tuning by Flare Rate

Update With Current Optimals

Figure 4. Settings Form in COMSOL Model Builder for efficient execution of the optimization studies and keeping track of optimal parameter values.

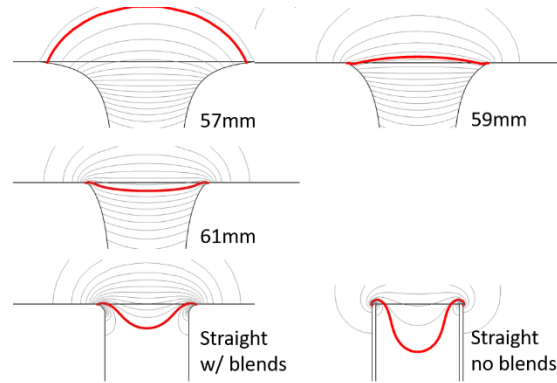


Figure 5. Velocity contours for ports with 3:1 aspect ratio of Length to D_c .

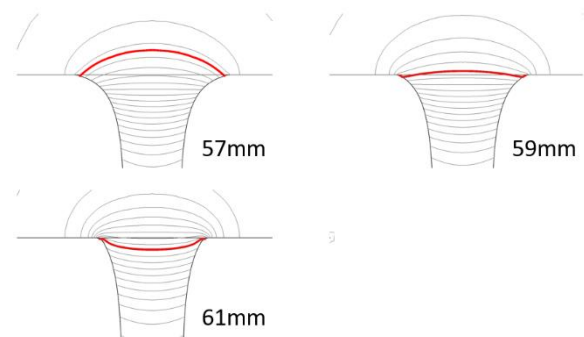


Figure 6. Velocity contours for ports with 4:1 aspect ratio.

Port Noise Measurements

The simulated port geometries were 3D printed and two medium density fiberboard enclosures were constructed in such a manner that they could hold two 10-inch drivers and a baffle that can mount to the reflective wall of the hemi-anechoic chamber of the Samsung Audio Lab.

A microphone fixture was mounted on the baffle to hold a G.R.A.S. 46 AM microphone at a distance of 10 cm from the port exits and angled at a 45° angle to protect the microphone from high pressure at the vortices. The test setup is shown in Figure 7.



Figure 7. Test box setup with two 10-inch drivers. Left: Box before mounting. Middle: Box with port mounted inside hemi-anechoic chamber. Left: View from outside hemi-anechoic chamber.

Table 2. Dimensions of ports with 3:1 and 4:1 aspect ratios.

Port	57 mm	59 mm	61 mm	Straight w/ blends	Straight no blends	57 mm	59 mm	61 mm
Aspect Ratio	3:1	3:1	3:1	3:1	3:1	4:1	4:1	4:1
Length [mm]	180	180	180	180	180	240	240	240
Dc [mm]	57	59	61	69	69	57	59	61
De [mm]	177	117	97	69	69	150	126	102
Rb [mm]	8.4	8.4	8.4	8.4	-	10.1	10.1	10.1
Vbox [L]	30.6	30.6	30.6	30.6	30.6	24.6	24.6	24.6

The 3:1 aspect ratio ports were driven with a multitone [14] signal that had a bandwidth of 20 Hz to 160 Hz. The voltage was stepped up from 1 V to 44 V, at which point the amplifier started to clip the signal. The frequency spectra measured for the 3:1 ports are shown in Figure 8. The plots clearly show how port “noise” develops around $f_p^1 \approx 950$ Hz at higher voltages.

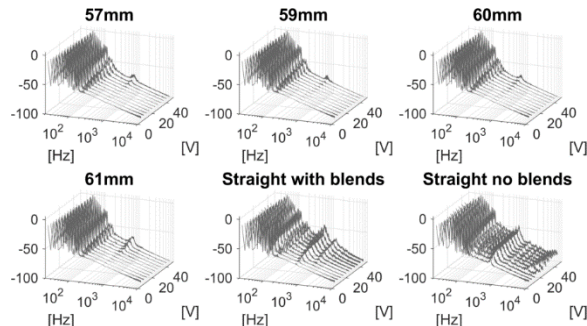


Figure 8. Normalized spectra for ports with 3:1 aspect ratio.

In order to better define a figure of merit for port noise, we plotted the spectral content at a bandwidth of one octave around f_p^1 , as a ratio to the total spectral content in Figure 9. The results clearly show how continuously-flared ports outperform the straight ports. The results also indicate that the onset of measurable noise for the 59-mm port happened at the highest voltage.

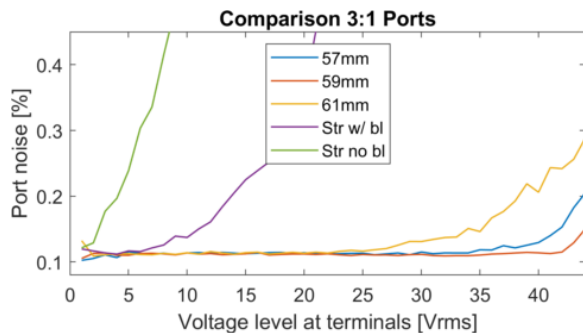


Figure 9. Port noise for ports with 3:1 aspect ratio as a function of drive level.

The 4:1 aspect ratio ports were driven with a sine tone of 40 Hz. The normalized spectra for the 4:1 ports are shown in Figure 10. Again the noise peak around $f_p^1 \approx 715$ Hz is clearly measurable. The figure of merit for port noise is shown in Figure 11.

The port noise measurements confirm the hypothesis that there is an optimal amount of flare rate for continuously-flared ports. Over- and under-flared ports create a stronger peak around f_p^1 . The onset of increasing output around f_p^1 happens at the highest drive level for optimally-flared ports.

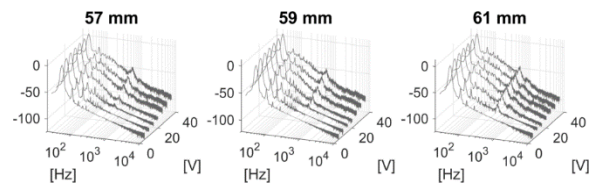


Figure 10. Output spectra for ports with 4:1 aspect ratio.

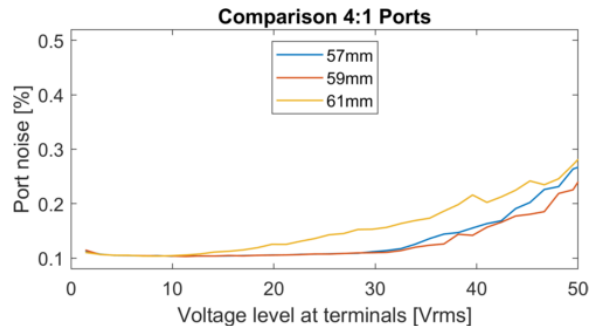


Figure 11. Port noise for ports with 4:1 aspect ratio as a function of drive level.

Listening Tests

Three double-blind listening tests were performed to validate the optimality of the simulated ports and correlate with the noise measurements. 15 listeners, ranging in age from 25 to 61 (mean = 40, SD = 12), participated in the first two listening tests with the 3:1 aspect ratio ports.

Preference Test with 3:1 Aspect Ratio Ports

Three different signals were recorded using the five 3:1 aspect ratio ports at four different voltage levels (4 V, 20 V, 40 V, 60 V). The three signals were synthesized sounds of a whale drum, a kick drum, and a bass guitar. All signals had fundamentals at 40 Hz. This resulted in a set of 12 factors (3 tracks, 4 voltages), and each combination of tracks and voltages had two repeats for a total of 24 trials. The 24 trials were played through headphones in a randomized order and all tracks were loudness normalized. Listeners used a custom software on a tablet graphical interface with five sliders to rate each port between 0 (strongly dislike) to 100 (strongly like) for each combination of factors.

There was a significant trend for listeners to prefer the 59-mm port at the higher voltages, particularly at 40 V. The straight port tubes received low ratings across all voltage levels, even at the lowest level of 4 V. Statistical details on the test results are published in [9] and the overall result of the port preference test is shown in Figure 12.

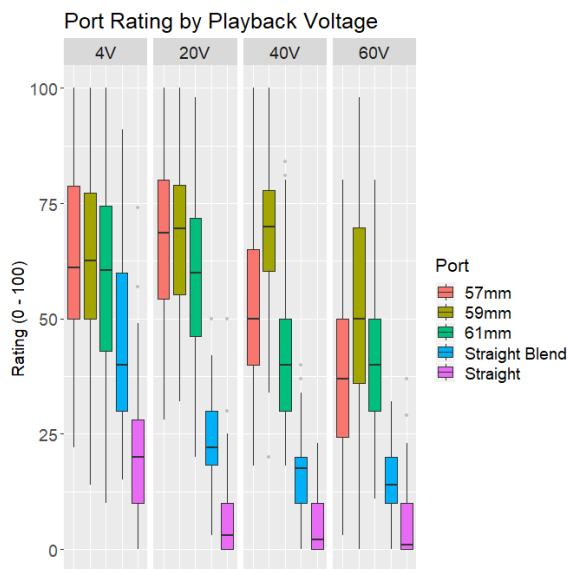


Figure 12. Overall port ratings by drive level for the 3:1 aspect ratio ports.

Method of Adjustment (MoA) Test with 3:1 Aspect Ratio Ports

In a second test, the same 15 listeners were asked to compare the noise of individual ports, recorded at different drive levels, to a reference recording. The reference recording was the whale drum track of the 59-mm port at 52 V. This reference was chosen, because the 59-mm port started to generate a small but discernable amount of noise. Random recordings of the five ports at different drive levels between 4 V

and 110 V were normalized for loudness and played through headphones. The listeners could toggle between the reference recording and the test recording. They were then asked to use a rotary knob to adjust the drive level of the test recording until the amount of noise was similar to the amount of noise they heard in the reference recording.

The results of the MoA test are shown in Figure 13, and they show that the 59-mm port was significantly less noisy and required at least 8 V (1.5 dB) more drive level (based on medians) to produce a similar amount of audible when compare to the over- and under-flared 57-mm and 59-mm ports. The straight ports need to be played at least 10 dB (36 V) less loud to match the reference noise level. The results also show that listeners were pretty good at picking the proper drive level for the 59-mm port to match the reference recording. This indicates that the test was performed well and the test was relatively easy.

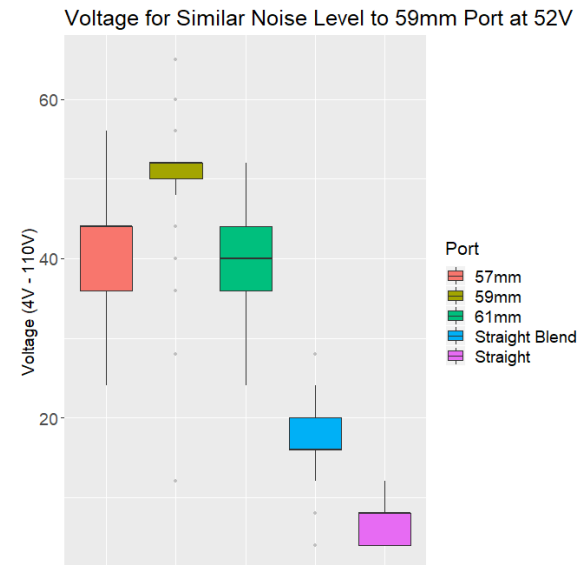


Figure 13. Results of the MoA test with 3:1 aspect ratio ports. Selected levels at which port noise was equal to the noise of port 59 mm at 52 V.

MoA test with 4:1 Aspect Ratio Ports

A similar MoA test was run with the three 4:1 aspect ratio ports. For this test we used near-field recordings of half-second sine bursts at 40 Hz at drive levels between 1 V and 40 V. When played back through headphones, the playback level was normalized by drive level. Seven listeners participated in this test, and the results are shown in Figure 14. On average the 61-mm port need to be played 4 V (1.1 dB) less loud to match the noise level of the 59-mm port, and the 57-mm port needed to be played 3 V (0.8 dB) less loud than the 59-mm port. The very wide distribution

of the 61-mm port is assumed to stem from the fact that the 61-mm port had an additional audible distortion that was not related to blowing noises. Again, listeners consistently picked the correct drive level for the reference 59-mm port.

Conclusions

This work shows how optimal designs of loudspeaker port tubes can be achieved with linear acoustic simulations in COMSOL by minimizing the curvature of the particle velocity contours at port exit. The efficient calculation of the acoustic Helmholtz equation lends itself much better for numerical optimization, rather than having to solve the numerically very expensive NS equations for fully resolved turbulence problems. Optimality of the designs was validated with measurements in anechoic chambers and double-blind listening tests. For ports with nominal Dc of 60 mm, a 2-mm (3.3%) change in central diameter results in performance hits of 0.8 to 3 dB. Straight ports perform at least 10 dB worse than optimally flared ports.

References

1. Salvatti, A., Devantier, A., and Button, D. J., "Maximizing performance from loudspeaker ports," *Journal of the Audio Engineering Society*, **50**(1-2), pp. 19–45, (2002)
2. Backman, J., "The nonlinear behavior of reflex ports," in *Audio Engineering Society Convention 98*, Paris, (1995)
3. Vanderkooy, J., "Loudspeaker Ports," in *Audio Engineering Society Convention 103*, New York City, (1997)
4. Vanderkooy, J., "Nonlinearities in Loudspeaker Ports," in *Audio Engineering Society Convention 104*, Amsterdam, (1998)
5. Roozen, N. B., Bockholts, M., van Eck, P., and Hirschberg, A., "Vortex sound in bass-reflex ports of loudspeakers. Part I. Observation of response to harmonic excitation and remedial measures," *The Journal of the Acoustical Society of America*, **104**(4), pp. 1914–1918, (1998)
6. Roozen, N. B., Bockholts, M., van Eck, P., and Hirschberg, A., "Vortex sound in bass-reflex ports of loudspeakers. Part II. A method to estimate the point of separation," *The Journal of the Acoustical Society of America*, **104**(4), pp. 1919–1924, (1998)
7. Roozen, N. B., Vael, J. E. M., and Nieuwendijk, J. A., "Reduction of Bass-Reflex Port Non-linearities by Optimizing the Port Geometry," in

- Audio Engineering Society Convention 104*, Amsterdam, (1998)
8. Rapoport, Z. and Devantier, A., "Analysis and Modeling of the Bi-Directional Fluid Flow in Loudspeaker Ports," in *Audio Engineering Society Convention 117*, San Francisco, (2004)
9. Bezzola, A., Devantier, A., and McMullin, E., "Loudspeaker Port Design for Optimal Performance and Listening Experience," accepted for *Audio Engineering Society Convention 147*, New York City, (2019)
10. Backman, J., "Fluid dynamics analysis of ported loudspeakers," in *Audio Engineering Society Convention 141*, Los Angeles, (2016)
11. Backman, J., "Nonlinearity of ported loudspeaker enclosures," in *Audio Engineering Society Convention 142*, Berlin, (2017)
12. Garcia-Alcaide, V. M., Palleja-Cabre, S., Castilla, R., Gamez-Montero, P. J., Romeu, J., Pamies, T., Amate, J., and Milan, N., "Numerical study of the aerodynamics of sound sources in a bassreflex port," *Engineering Applications of Computational Fluid Mechanics*, **11**(1), pp. 210–224, (2017)
13. Bezzola, A., "Numerical Optimization Strategies for Acoustic Elements in Loudspeaker Design", in *Audio Engineering Society Convention 145*, New York City, (2018)
14. Brunet, P., "Use of Repetitive Multitone Sequences to Estimate Nonlinear Response of a Loudspeaker to Music", in *Audio Engineering Society Convention 143*, New York City, (2017)

Acknowledgements

Samsung Electronics and Samsung Research America supported this work. The author would like to thank the entire staff of Samsung's US Audio Lab who helped with all aspects of this research, offered insightful suggestions, and contributed to this work.